Optical Nanotrapping Using Illuminated Metallic Nanostructures: Analysis and Applications

E. P. Furlani, A. Baev and P. N. Prasad

The Institute for Lasers, Photonics and Biophotonics, University at Buffalo SUNY
432 Natural Sciences Complex
Buffalo, NY 14260-3000
efurlani@buffalo.edu,

ABSTRACT

We present a theoretical study of plasmonic-based optical trapping of neutral sub-wavelength particles in proximity to illuminated metallic nanostructures. We compute the dipolar force on the particles using 3D full-wave electromagnetic analysis, and we perform parametric studies of the force as a function of nanostructure geometry, particle size, and field polarization. We discuss advantages and applications of plasmonic nanotrapping.

Keywords: optical nanotrapping, optical nanoparticle manipulation, plasmonic nano-tweezers, plasmonic-enhanced optical manipulation

1 INTRODUCTION

The interest in optical manipulation continues to grow, especially for biological applications where the manipulated objects include viruses, cells and intracellular organelles [1-5]. While micron and sub-micron particles can be manipulated using conventional laser tweezers, the resolution of this approach is diffraction-limited (~250 nm), and the high optical power and focusing of the laser beam can limit the exposure time of a trapped specimen. An alternate trapping method that overcomes these limitations involves the use of plasmonics [6-7]. Specifically, sub-wavelength particles can be manipulated and trapped using the enhanced near-field gradients that exist around illuminated metallic nanostructures. To date, various groups have conducted theoretical studies of plasmonic-based optical trapping involving a metal tip, nanoaperture, and apertureless probe [8-11]. Parallel and selective optical trapping has been demonstrated experimentally using an ordered array of Au disks [12].

The optical force produced by metallic nanostructures can be used to control dielectric or metallic nanoparticles, which can be functionalized to bind with a target biomaterial thereby enabling optical manipulation of nanoscale bioparticles. Plasmonic nano-manipulation holds potential for a number of diverse applications including nanoparticle chemistry, nanorheology, nanoscale bioseparation, ultra-sensitive biosensing, and Lab-on-a-Chip devices.

In this paper we discuss plasmonic-based optical trapping of dielectric nanoparticles in proximity to illuminated metallic nanopillars and nanorings (Fig. 1a). We perform a theoretical study of the dipolar force on particles using 3D full-wave electromagnetic analysis. We consider 2 and 4 nanopillar configurations, and nanoring structure with and without a central plasmonic nanopillar.

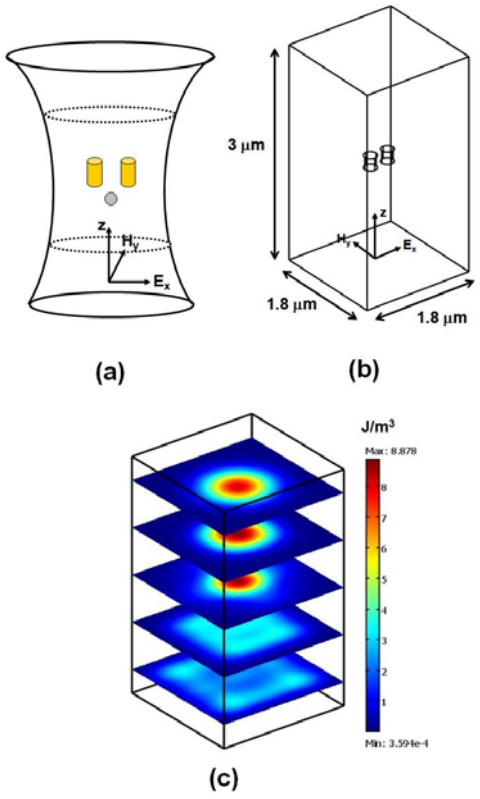

Figure 1: Plasmonic optical manipulation: (a) physical model – a dielectric nanoparticle beneath two metallic nanopillars; (b) the FEA computational domain; (c) time-averaged electric energy density showing focusing at center of computational domain – no pillars present.

We compute the force as a function of the nanopillar configuration, the particle size, and the polarization of the incident field. It should be noted that while the results presented here are theoretical, optical manipulation using an array of tapered nanopillars has been demonstrated in the laboratory wherein the controlled motion of microbubbles in an immersion oil has been achieved with sub-micron precision [13-14].

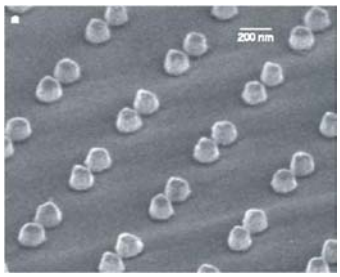

Figure 2: Fabricated array of tapered gold nanopillars (adapted from [14]).

2 ANALYSIS AND RESULTS

We use 3D full-wave time-harmonic finite element analysis (FEA) to study the optical field and dipolar force distribution produced by gold nanopillars and nanorings. We use the COMSOL Multiphysics FEA-based electromagnetic solver for our numerical analysis. The computational domain spans 3 μm in the direction of propagation (z-axis), and 1.8 μm in both the x and y directions (Fig. 1b). We study various nanopillar and nanoring configurations, and for each of these we compute the field and force distribution as a function of geometrical spacing, particle size, and field polarization. In all cases the nanostructures are centered height wise along the z-axis in the computational domain,

We illuminate the nanopillars/nanorings in free-space from below with a uniform plane wave at an optical wavelength λ = 532 nm. The incident field has a prescribed magnitude $|E| = 1\times10^6$ V/m, which corresponds to a CW power of 4 mW. This condition is imposed at the lower boundary (at z = -1.5 μm). We apply scattering (low reflection) boundary conditions at the top of the computational domain (z = 1.5 μm), and at the boundaries perpendicular to the E field (x = y = ± 0.9 μm). The incident field is effectively apertured by the finite x-y cross-section of the computational domain at the lower boundary, and this focuses the field at the center of the computational domain (z = 0) as shown in Fig. 1c. Thus, the field is focused at the center of the nanopillar structure.

We analyze the optical trapping of sub-wavelength particles by computing the time-averaged dipolar force,

$$\langle F_i \rangle = \frac{1}{2}\sum_j \mathrm{Re}\left[\alpha E_{0j}\partial^i \left(E_{0j}\right)^*\right], \qquad (1)$$

where E_{0j} $(j = 1,2,3)$ are the Cartesian components of the optical field, and

$$\alpha = \frac{4\pi\alpha_0\varepsilon_0}{\left[1-\alpha_0\left(\frac{k^2}{a}-\frac{2}{3}ik^3\right)\right]} \qquad (2)$$

is the polarizability of the particle, where $\alpha_0 = R_p^3\frac{\varepsilon_r-1}{\varepsilon_r+2}$. R_p and ε_r are the radius and relative permittivity of the particle, respectively [15]. The imaginary term in α accounts for the scattering force on a particle, and it is important to note that the sign of this term (i.e. $\pm\frac{2}{3}ik^3$) depends on the convention used in the time-harmonic analysis, i.e. $\exp(i\omega t)$ or $\exp(-i\omega t)$ [16-17]. The COMSOL program uses the former, which is compatible with Eq. (2).

We model the dielectric permittivity of the gold nanostructures using a Drude-like model with the following parameters: the bulk plasma frequency is $1.37\times10^{16}\,\mathrm{sec}^{-1}$, the damping frequency is $4.08\times10^{13}\,\mathrm{sec}^{-1}$, and the high-frequency limit term including contributions from interband transitions is 12.9. We study a variety of nanopillar and nanoring configurations that include a pair of nanopillars along the x-axis (Fig. 1b), a group of four nanopillars centered about the origin (Fig. 6a), and a nanoring with and without an isolated central metallic pillar (Fig. 8a).

2.1 Two Nanopillar System

We first consider a two nanopillar system in which the nanopillars are positioned along the x-axis as shown in Fig. 1a. We fix the dimensions of the nanopillars, radius = 100 nm and height = 200nm. We compute the field and force distribution as a function of pillar-to-pillar spacing, particle size, and field polarization. The time-averaged electric field intensities for TE and TM polarized fields are compared with TE free-space illumination in Fig. 3. These plots show that the nanopillars produce local field gradients that are polarization dependent. They also indicate that particles on the z-axis will be confined in a lateral sense, i.e. F_x and F_y act towards the axis. Plots of the TE and TM time-averaged axial force F_z along the z-axis vs. particle size are shown in Figs. 4a and 4b. The spacing between the pillars is 100 nm. Note that TE polarization (E along x-axis) produces stronger forces than TM polarization (E along y-axis). Particle trapping can occur where F_z changes sign, positive-to-negative, as shown in Fig. 4a. Note that for TM polarization there is no trapping for larger particles (e.g. for $R_p \geq$ 300 nm, Fig. 4b). This is because the scattering force, which is strictly positive, dominates the gradient force for larger particles. The optical force on a 100 nm

particle for TE and TM polarization compared to the free-space (scattering) force is shown in Fig. 5.

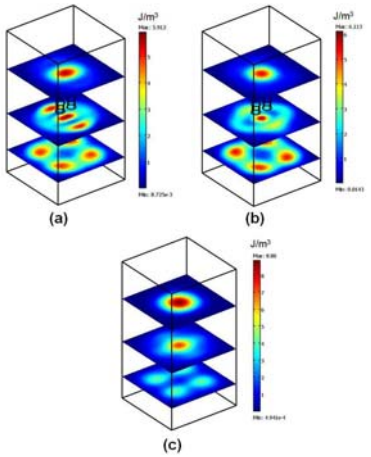

Figure 3: Two nanopillar system - time-averaged electric energy density at various planes: (a) TE analysis; (b) TM analysis; (c) TE analysis - free-space.

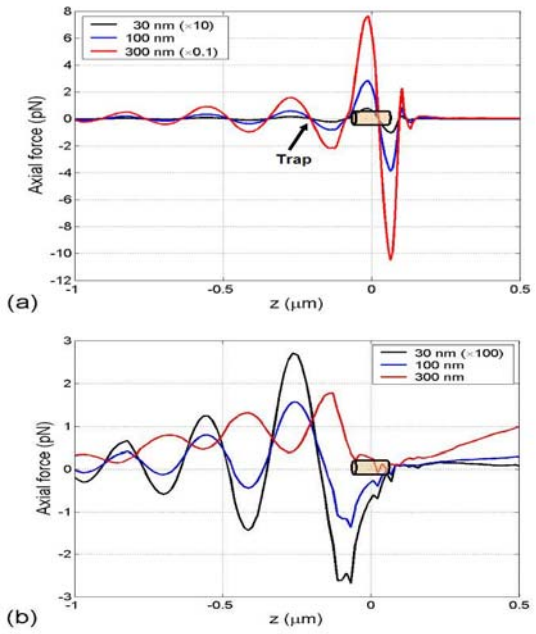

Figure 4: Two nanopillar system - time-averaged dipolar axial force vs. particle radius (a) TE analysis; (b) TM analysis.

2.2 Four Nanopillar System

Next, we study a four nanopillar system in which four gold nanopillars are positioned symmetrically about the axis as shown in Fig. 6a. The nanopillars are the same size as above. The time-averaged gradient force potential ($-|E|^2$) shown in Fig. 6b indicates lateral trapping along the z-axis.

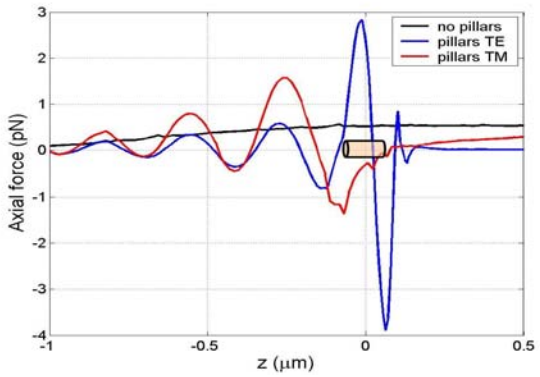

Figure 5: Two nanopillar system - axial force for 100 nm particle.

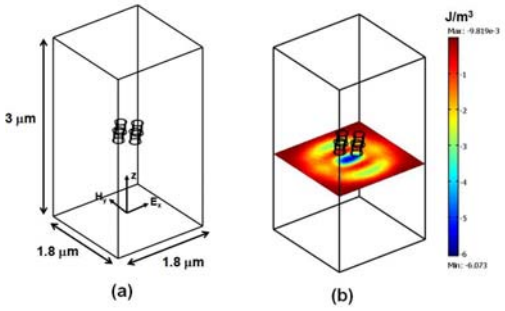

Figure 6: Four nanopillar system: (a) geometry; (b) time-averaged force potential.

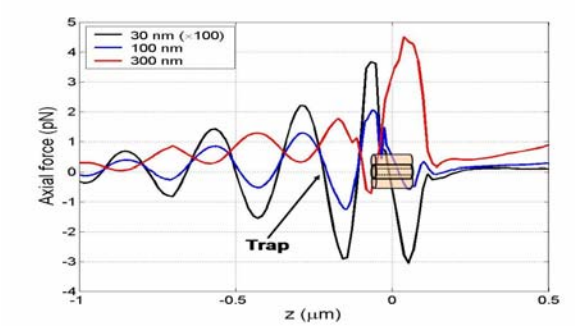

Figure 7: Four nanopillar system: FEA time-averaged dipolar force vs. particle radius.

F_z along the z-axis for different particles sizes is shown in Fig. 7. Note that smaller particles (e.g. R_p = 30, 100 nm) can potentially be trapped, but that larger particles ($R_p \geq$ 300 nm) can not.

2.3 Nanoring System

The last system we study consists of a gold nanoring centered about the origin. The ring has an outer diameter of 600nm and a height of 200 nm. We consider a range of inner diameters, with and without isolated central metallic

pillars of varying diameters. Figure 8 shows a nanoring with a 450 nm inner diameter surrounding an isolated central metallic pillar that is 100 nm in diameter. The time-

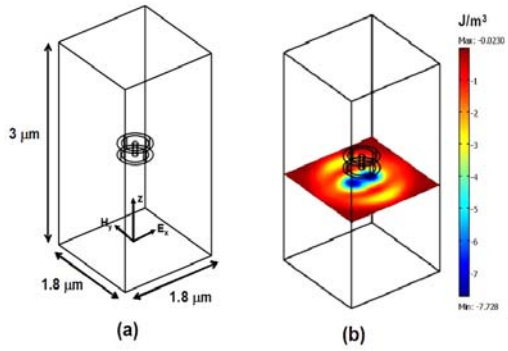

Figure 8: Nanoring analysis: (a) nanoring with a central metallic pillar; (b) dipolar gradient force potential 200 nm below the nanoring.

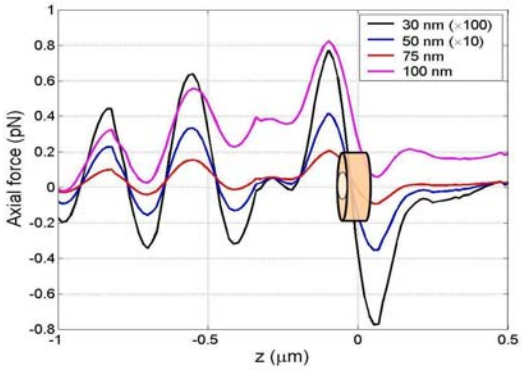

Figure 9: Nanoring system: time-averaged axial dipolar force vs. particle radius.

averaged gradient force potential for this geometry is shown in Fig. 8b. Note that there are two local minima in this plot, which are located along the x-axis on either side of central pillar. Particle trapping occurs at these points. The axial force vs. particle radius for a ring with a 450 nm inner diameter and without the central pillar is plotted in Fig. 9.

In summary, our analysis indicates that all of the nanostructures above provide pNs of trapping force at modest power levels. For the two nanopillar system, the magnitude of the force depends on the spacing of the nanopillars, and the polarization of the incident field. TE polarization and closer spacing produce stronger forces.

3 APPLICATIONS

Plasmonic-based optical manipulation holds potential for a variety of applications, especially in the fields of biophysics and biotechnology. Specific applications include (i), nanoscale size-sensitive bio-separation and filtering (ii) nanoscale biosensing, (iii) virus manipulation, (iv) cellular sorting and patterning, (v) manipulation for cellular microsurgery, (vi) nanobead-based single-molecule DNA sequencing, and (vii) characterization of single biopolymers [10].

4 CONCLUSIONS

Plasmonic-based optical trapping is its infancy and growing rapidly. Research in this area will significantly advance fundamental understanding in fields such as nanophotonics and biophotonics. Plasmonic optical trapping has advantages over conventional laser trapping in that it enables a higher spatial resolution, lower trapping energy, parallel trapping of multiple specimens, and a higher level of system integration, which is important for Lab-on-Chip applications. Novel plasmonic trapping structures and systems can be designed and optimized using commercial electromagnetic software, and this capability will facilitate the development of a new generation of systems for manipulating matter at the nanoscale.

ACKNOWLEDGEMENT

We acknowledge support from the Air Force Office of Scientific Research.

REFERENCES

[1] A. Ashkin, Proc. Natl. Acad. Sci. **94**, 4853, 1997.
[2] C. L. Kuyper and D. T. Chiu, Appl. Spectrosc. **56** (11) 295A, 2002.
[3] A. Ashkin and J. M. Dziedzic, Science **235**, 1517, 1987.
[4] K Svoboda and S. M. Block, Annu. Rev. Biophys. Biomol. Struct. **23,** 247 1994
[5] P. N. Prasad, Introduction to Biophotonics, John Wiley & Sons, NJ, 2003.
[6] H. A. Atwater, Scientific American **296,** 56, 2007.
[7] P. N. Prasad, Nanophotonics, John Wiley & Sons, NJ, 2004.
[8] L. Novotny, R. X. Bian, and X. S. Xie, Phys. Rev. Lett. **79**, 645, 1997.
[9] K. Okamoto and S. Kawata, Phys. Rev. Lett. **83**, 4534, 1999.
[10] P. C. Chaumet, A. Rahmani, and M. Nieto-Vesperinas, Phys. Rev. Lett. **88**, 123601, 2002.
[11] X. Miao and L. Y. Lin, IEEE J. Sel. Top. Quant. Elec. **13**, 1655, 2007.
[12] M. Righini, A. S. Zelenina, C. Girard and R. Quidant, Nature Physics **3**, 477, 2007.
[13] A. R. Sidorov, Y. Zhang, A. N. Grigorenko and M. R. Dickinson, Opt. Comm. **278,** 439, 2007
[14] A. N. Grigorenko, A. K. Geim, H. F. Gleeson, Y. Zhang, A. A. Firsov, I. Y. Khrushchev and J. Petrovic, Nature **438,** 335, 2005.
[15] P. C. Chaumet and M. Nieto-Vesperinas, Opt. Lett. **25**, 1065, 2000.
[16] J. I. Hage and J. M. Greenberg, Astrophys. J. **361**, 251, 1990
[17] Private communication with P. C. Chaumet.